Proceedings of ISROMAC-11:
International Symposium on Transport Phenomena and Dynamics of Rotating Machinery
February 26 - March 2, 2006, Honolulu, Hawaii USA

ONE-DIMENSIONAL MODELING OF ROTOR STATOR INTERACTION IN FRANCIS PUMP-TURBINE

Christophe Nicolet
EPFL Ecole polytechnique fédérale de Lausanne
Laboratory for Hydraulic Machines,
33 bis, av. de Cour, CH-1007 Lausanne,
Switzerland
christophe.nicolet@epfl.ch

Nicolas Ruchonnet
EPFL Ecole polytechnique fédérale de Lausanne
Laboratory for Hydraulic Machines,
33 bis, av. de Cour, CH-1007 Lausanne,
Switzerland

François Avellan
EPFL Ecole polytechnique fédérale de Lausanne
Laboratory for Hydraulic Machines,
33 bis, av. de Cour, CH-1007 Lausanne,
Switzerland

KEYWORDS

Hydroacoustic modeling, rotor stator interaction, pump turbine.

ABSTRACT

A one-dimensional hydroacoustic model is set up to perform the numerical simulation of the rotor-stator interaction of a Francis pump-turbine scaled model. The numerical results enable to identify both rotating diametrical modes in the vaneless gap between the 20 guide vanes interacting with the 9 rotating impeller blades and the standing waves in the spiral casing. Moreover, the simulations enlighten the interaction between these rotating diametrical modes and the standing waves. Finally, the parametric study of the influence of the guide vane thickness, the wave speed and rotational speed emphasizes the predominant role of the eigen frequencies of the hydraulic system.

INTRODUCTION

Hydraulic pump-turbine operating under steady state conditions are subject to pressure fluctuations resulting from the interaction of the rotating parts and the stationary parts of the machine. This Rotor-Stator Interaction, RSI, are the consequence of the interaction between the rotating flow perturbations so-called potential flow perturbations caused by the impeller blades and the flow perturbation caused by the guide vanes. This interaction induce pressure waves propagating in the entire hydraulic machine. As a result the RSI phenomena may cause two different kinds of pressure fluctuations in the machine:

- diametrical pressure mode rotating in the vaneless gap between the guide vane and the impeller blades as described by Bolleter [1] and Tanaka et al. [13];
- standing waves in the spiral casing as described by Chen [2] and Dörfler [4].

The first phenomenon may cause hydromechanics resonance between the rotating diametrical pressure mode and the structure of impeller [15] or of the head cover [6] and may induce strong vibrations, noise, fissures or guide vanes bearing ruins. The second phenomenon may cause resonance with the power house structure that generates unacceptable vibrations and noise [13]. The standing wave phenomenon may affect also the penstock [4], [3] which evidences the potential interaction of the hydraulic machine with the hydraulic circuit.

The prediction of such phenomena is a challenging task during the early stage of the design of a reversible pump turbine

unit for a hydroelectric power plant. Some analytical models have been developed by Bolleter [1] and Tanaka et al. [13] for the diametrical mode shape and by Chen [2] and Dörfler [4] for the standing wave allowing for the prediction of the risk of occurrence of these phenomena. The prediction of the occurrence of the standing wave is based on the analysis of the traveling time of pressure waves propagating in a one-dimensional system modeling the pump turbine accordingly to its topology. Recently, Haban et al. [8] have developed more sophisticated one-dimensional models based on matrix transfer method that have shown their capability of predicting spiral casing standing wave patterns. By the use of such models Fischer et al. [6] have pointed out the link between the standing waves in the spiral casing and the penstocks and the diametrical pressure mode rotating in the vaneless gap by performing a forced response analysis in the frequency domain. However this approach requires the identification of the excitation pattern by the method described by Bolleter [1] and Tanaka et al. [13].

The simulation of the incompressible 3D unsteady flow of a vaneless centrifugal pump performed by Gonzalez et al. [7] using commercial CFD tool has shown the capability of CFD to predict accurately the unsteady convective field related to the RSI phenomenon at the blade passing frequency which is dominant close to the nominal operating point. However some discrepancies appeared for off-design operating conditions where acoustic behavior becomes more effective due to a blade-tongue interaction. Such an incompressible code cannot account for the propagating part of the flow which may lead to standing wave phenomenon. Therefore the separation of hydraulic and acoustic pressure fluctuations by means of least-squares residual method developed by Morgenroth [9] was used. A model accounting for both the jet-wake pattern of the convective flow and for the blade-tongue interaction has been set up by Parrondo et al. [12]. Through an experimental identification of the parameters of acoustic model a good agreement has been found between the model and the measurements even for off-design operating conditions where the amplitude of the blade-tongue interaction was found to have 10 times the amplitudes of the wake jet part of the flow.

To be able to predict the amplitudes of the pressure fluctuations resulting from RSI it appears that combination of unsteady incompressible RANS model and 1D acoustic model is a suitable approach. This approach would leads to a RSI computing methodology for the prediction of pressure amplitudes where the unsteady incompressible RANS calculation accounts for the rotor stator excitation mechanism considering all the parameters; i. e. vaneless gap, impeller blade angle, guide vane opening, jet-wake effect, etc. The first step of this approach is to set up a hydroacoustic model of a pump turbine and to investigate RSI patterns and perform a sensitivity study of the model.

This paper aims to present the numerical simulation of the hydroacoustic part of the RSI phenomenon based on a one-dimensional hydroacoustic model. Therefore the case of 20 guide vanes and 9 impeller blades high head Francis pump turbine is investigated. First the RSI patterns of the pump turbine are described. Then the mathematical model implemented in the software SIMSEN is briefly presented. The determination of the pump turbine hydroacoustic parameters is described. The RSI excitation is modeled by a valve network driven accordingly to the spatial and temporal evolution of the flow distribution between the stationary and the rotating parts of the machine. The results obtained by the simulations in time domain evidences the RSI patterns of the pump turbine of interest. A parametric study is presented and influence of blade thickness, wave speed and the rotational speed is investigated.

NOMENCLATURE

A = Cross Section Area, m^2

C = Absolute Mean Flow Speed, m/s, $C = Q/A$

C_h = Hydraulic Capacitance, m^2, $C_h = gA/a^2$

D = Pipe diameter, m

E = Young Modulus, Pa

E = Machine Specific Energy, J/kg, $E = gH_1 - gH_2$

H = Head, m, $H = E/g$

L_h = Hydraulic Inductance, s^2/m^2, $L_h = dx/gA$

Q = Flow rate, m^3/s $Q = C \cdot A$

R_h = Hydraulic Resistance, s/m^2,
$$R_h = \lambda dx|Q|/2gDA^2$$

R_{ref} = Machine Reference Radius, m

h = Piezometric Head, m, $h = p/\varpi + Z$

a = Wave Speed, m/s

f_b = Impeller Rotational Frequency, Hz

p = Pressure, Pa.

g = Gravity Acceleration, m/s^2

ϖ = Specific Weight, kg/m^{2}s^2, $\varpi = \rho g$

ρ = Water Density, kg/m^3

φ = Discharge Coefficient, $\varphi = Q/\pi\omega R_{ref}^3$

ψ = Specific Energy Coefficient, $\psi = 2E/\omega^2 R_{ref}^2$

ν = Machine Specific Speed, $\nu = \varphi^{1/2}/\psi^{3/4}$

λ = Local Loss Coefficient

ω_b = Impeller Angular Speed, rad/s

n = Harmonic Order

m = Harmonic Order

z_o = Number of Guide Vanes, $z_o = 20$

z_b = number of impeller blades, $z_b = 9$

θ_s = Angle in the Stationary System

θ_r = Angle in the Rotating System

B_n = Amplitude for the n[th] Harmonic, Pa.

B_m = Amplitude for the m[th] Harmonic, Pa

ϕ_n = Phase for the n[th] Harmonic

ϕ_m = Phase for the m[th] Harmonic

RSI PATTERNS IN FRANCIS PUMP TURBINE

The flow field leaving the guide vane of a Francis pump turbine in generating mode is characterized by the velocity defect caused by the guide vanes. The pressure field attached to the rotating impeller blade induces also incoming flow field distortions. No matter how complex are these two periodic flow fields they can be expressed as Fourier series. Then, both the stationary and rotating pressure fields can be expressed as:

$$p_s(\theta_r, t) = \sum_{n=1}^{\infty} B_n \cos\left(nZ_0\theta_r + \phi_n\right) \qquad (1)$$

$$p_r(\theta_r, t) = \sum_{m=1}^{\infty} B_m \cos\left(mZ_b \cdot \theta_r + \phi_m\right) \qquad (2)$$

The resulting pressure field, combining the guide vanes and the impeller blade pressure field is characterized by a strong modulation process as illustrated Figure 1. The pressure in the area of the vaneless gap between the guide vanes and impeller blades can therefore be expressed as the product of both rotating and stationary fields of pressure leading to the summation of every p_{mn} component:

$$p_{mn}(\theta, t) = A_{mn} \cos\left(nZ_o \cdot \theta_s + \phi_n\right) \cdot \cos\left(mZ_b \cdot \theta_r + \phi_m\right) \quad \text{for } n = 1, 2, \ldots\infty \text{ and } m = 1, 2, \ldots\infty \qquad (3)$$

where A_{mn} is the combined pressure amplitude due to the interaction of each harmonics [13].

By using the well known identity for circular functions: Eq.(3) can be expressed as:

$$p_{mn}(\theta_s, t) = \frac{A_{mn}}{2} \cos\left(nZ_o \cdot \theta_s - mZ_b \cdot \theta_r + \phi_n - \phi_m\right) + \frac{A_{mn}}{2} \cos\left(nZ_o \cdot \theta_s + mZ_b \cdot \theta_r + \phi_n + \phi_m\right) \qquad (4)$$

Moreover, the impeller angle coordinate is related to the stationary system of reference as $\theta_r = \theta_s - \omega t$, then the pressure field in the stationary coordinates becomes:

$$p_{mn}(\theta_s, t) = \frac{A_{mn}}{2} \cos\left(mZ_b\omega t - \left(mZ_b - nZ_o\right)\theta_s + \phi_n - \phi_m\right) + \frac{A_{mn}}{2} \cos\left(mZ_b\omega t - \left(mZ_b + nZ_o\right)\theta_s - \phi_n - \phi_m\right) \qquad (5)$$

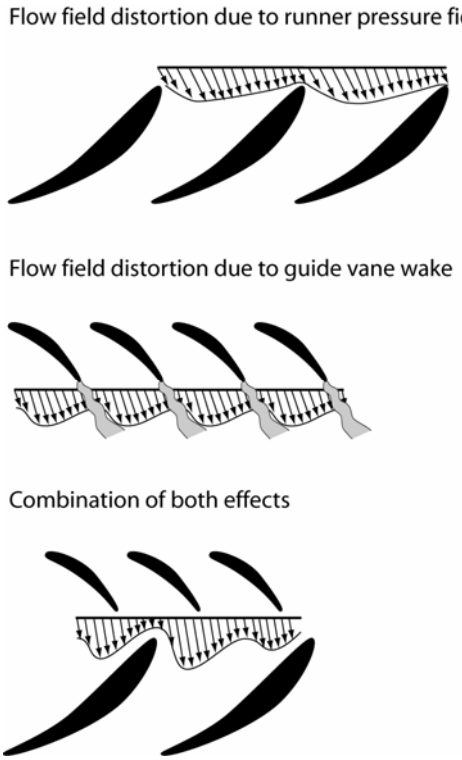

Figure 1 : Modulation process between impeller blade flow field and guide vanes flow field.

This equation describes the RSI pressure field in the vaneless gap which is function of time and space [5]. This pressure field represents 2 diametrical pressure modes having the following numbers of minima and maxima :

$$k_1 = m \cdot Z_b - n \cdot Z_o \text{ and } k_2 = m \cdot Z_b + n \cdot Z_o \qquad (6)$$

rotating with the respective spinning speed in the stationary frame of reference.

$$\omega_1 = mZ_b\omega_b / k_1 \text{ and } \omega_2 = mZ_b\omega_b / k_2 \,. \qquad (7)$$

Furthermore, the sign of the diametrical mode numbers k_1 and k_2 indicates that the diametrical mode is rotating in the same direction as the impeller when positive and counter-rotating when negative. It is also important to notice that lower amplitudes are expected for higher k values, because of the high harmonic number. As a result, k_2 is usually not relevant. The Figure 2 presents an illustration of the meaning of the k values.

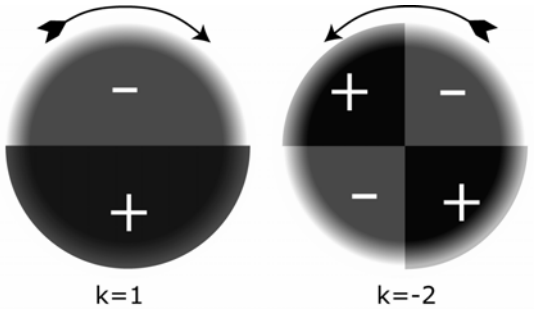

Figure 2 : Diametrical modes shapes representation according to k values.

The pump turbine of interest is a scale model of pump turbine which has a specific speed of $\nu = 0.17$, 20 guide vanes, 9 impeller blades and an outlet diameter (turbine mode) of $R_{le} = 400\ \text{mm}$. According to this rotor-stator blade arrangement the RSI patterns of this pump turbine are determined analytically using relations (5), (6) and (7), see Table 1.

				Stationnary frame			Rotating frame		
n	m	k1	k2	ω1/ωb	ω2/ωb	f/fb	ω1'/ωb	ω2'/ωb	f/fb
		mZb-nZo	mZb+nZo	mZb/k1	mZb/k2	mZb	nZo/k1	nZo/-k2	nZo
1	2	-2	38	-9.0	0.5	18	-10.0	-0.5	20
1	3	7	47	3.9	0.6	27	2.9	-0.4	20
2	4	-4	76	-9.0	0.5	36	-10.0	-0.5	40
2	5	5	85	9.0	0.5	45	8.0	-0.5	40

Table 1 : RSI patterns of the pump turbine ($Z_o = 20$; $Z_b = 9$).

Table 1 points out the 4 diametrical rotating modes shapes that may present high amplitudes, it is for $k_1 = -2, 7, 5, -4$ with the corresponding frequencies in the stationary frame $f/f_b = mZ_b = 18, 27, 36$ and 45. In the rotating frame of reference these frequencies reduced to $f/f_b = mZ_o = 20$ for the first 2 modes and $f/f_{bo} = 40$ the second 2 modes.

HYDROACOUSTIC MODELING OF FRANCIS PUMP TURBINE

Hydroacoustic modeling

By neglecting the convective terms $C\partial/\partial x$ and assuming plane pressure wave and uniform velocity field in a cross section, the momentum and the continuity equations established for the pipe of a length dx, a cross section A and a wave speed a, Figure 3, reduces to the simple hyperbolic partial differential equations see [16] :

$$\begin{cases} \dfrac{\partial h}{\partial t} + \dfrac{a^2}{gA} \cdot \dfrac{\partial Q}{\partial x} = 0 \\ \dfrac{\partial h}{\partial x} + \dfrac{1}{gA} \cdot \dfrac{\partial Q}{\partial t} + \dfrac{\lambda |Q|}{2gDA^2} \cdot Q = 0 \end{cases} \tag{8}$$

Where the h and Q variables are respectively the piezometric head and the discharge expressed as:

$$h = z + p/(\rho \cdot g) \qquad Q = C \cdot A \tag{9}$$

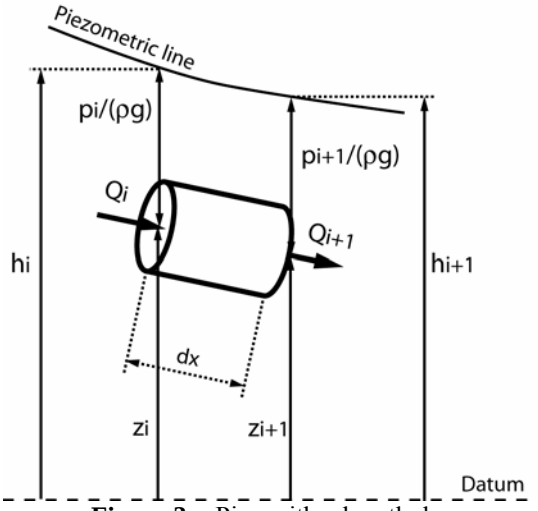

Figure 3 : Pipe with a length dx.

The system of hyperbolic equations (8) is solved using Finite Difference Method considering a 1st order centered scheme discretization in space and a scheme of Lax for the discharge. This approach leads to a system of ordinary differential equations that can be represented as a T-shaped equivalent scheme as presented Figure 4. The RLC parameters of this equivalent scheme are given by:

$$R_h = \frac{\lambda \cdot |\overline{Q}| \cdot dx}{2 \cdot g \cdot D \cdot A^2} \qquad L_h = \frac{dx}{g \cdot A}$$
$$C_h = \frac{g \cdot A \cdot dx}{a^2} \tag{10}$$

Here λ is the friction coefficient. The hydraulic resistance R_h, the hydraulic inductance L_h, and the hydraulic capacitance C_h correspond respectively to losses, inertia and storage effects.

The model of pipe with a length L is made of a series of n_b elements based on the equivalent scheme of Figure 4. The system of equations relative to this model is set-up using Kirchoff laws. Time integration of the full system is achieved by a Runge-Kutta 4th order procedure.

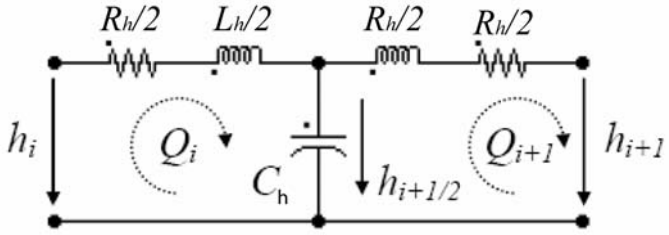

Figure 4 : Equivalent scheme of a pipe.

All the procedures for building up, solving and anaylsisng the hydroacoustic model of the whole system are implemented within the in house code SIMSEN [10]. Moreover, SIMSEN provides a complete object library including both

electrotechnical, control and hydraulic components such as valve, surge tanks, turbines.

Pump turbine hydroacoustic model

The plan view of the 20 guide vanes and 9 blades Francis pump turbine scale model of interest is presented Figure 5. The hydroacoustic model of this pump turbine is made of a pipe network, Figure 6..

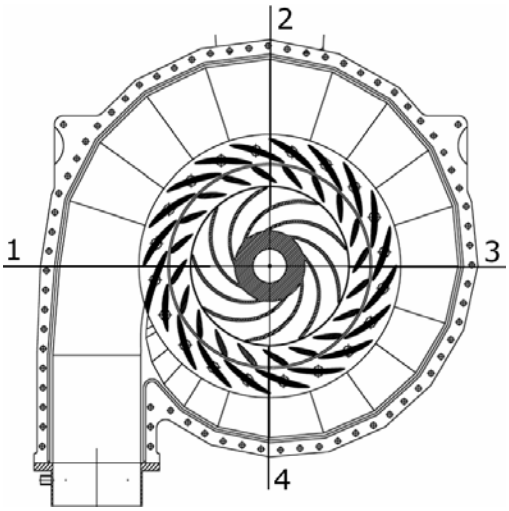

Figure 5 : Plan view of the pump turbine.

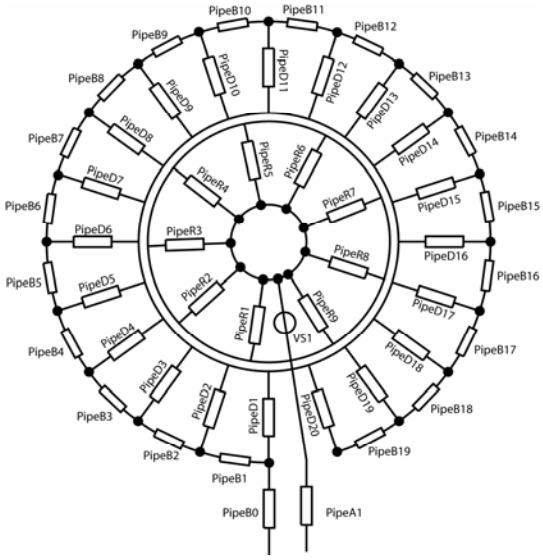

Figure 6 : Hydroacoustic model of the pump turbine.

The hydroacoustic model is made of 20 pipes for the guide vanes (pipes D1 to D20), 9 pipes for the impeller (pipes R1 to R9) as well as 19 pipes for the spiral casing (pipes B1 to B19). The first part of the spiral casing between the turbine inlet and the guide vane N°1 is modeled by the pipe B0. The diffuser of the pump turbine is modeled by the pipe A1. The energy transfer through the impeller is modeled by the pressure "source" VS1 which head is function of discharge H=H(Q) according to the slope of the pump turbine characteristics linearized around the operating point of interest. The connection between the stationary part and the rotating part is achieved through 180 valves connecting each guide vane to each impeller vane. The 180 valves are controlled by the flow distribution between the stationary part and the rotating part according to the impeller angular position $\theta(t)$ The valve head loss is calculated to ensure the idealized discharge evolution presented Figure 7.

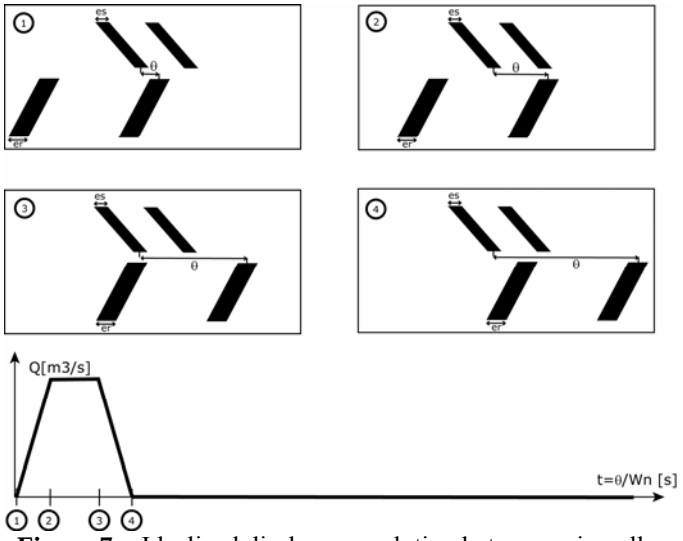

Figure 7 : Idealized discharge evolution between a impeller vane and a guide vane as function of the spatial coordinate of the impeller θ.

Assuming a constant impeller speed the discharge evolution between one guide vane and one impeller vane is function of the connection area between them. During the rotation of the impeller 4 phases are identified:

- phase 1: the impeller blade start to pass in front of the first blade of a guide vane, the discharge between the guide vane and the impeller vane increases linearly accordingly to the connection area increase until the impeller blade reaches the second blade of the guide vane;
- phase 2: the discharge between the guide vane and the impeller vane remains constant until the second impeller blade reaches the first blade guide vanes, the connection area being constant;
- phase 3: the discharge between the guide vane and the impeller vane decreases linearly according to the connection area decrease;
- phase 4: the discharge between the guide vane and the impeller vane is kept to zero as the connection area is zero until the phase 1 is reached again.

The discharge evolution described above acts like a sliding slot between the 20 guide vanes and one impeller vane. As a result there are 9 slots for the full pump turbine, one for each impeller vane. Each slot angle being shifted by $2\pi/Z_o$. The discharge law can be modified in order to take into account the thickness of both the guide vanes and impeller blades, e_o and e_b respectively. The thickness can be expressed as equivalent

angle measured in degrees at the vaneless gap radius. For the first part of investigations of this paper, the thickness of the impeller blades is taken arbitrary equal to 4°, the real one being 3°. The consideration of the blades thickness induces discontinuity in the overall discharge law. It means that the point 3 of the discharge law of an impeller blade does not correspond to the point 2 of the following impeller blade but is shifted of the value of e_b. The lack of discharge between two consecutives impeller blades is the source of the excitation mechanism of this RSI model.

HYDROACOUSTIC PARAMETERS DETERMINATION

For the determination of the RLC terms of the hydroacoutic model of a pipe the following values must be determined for each pipe:

- the length L;
- the cross section area A;
- the friction coefficient λ;
- the wave speed a.

The determination of the length and cross section has been done using the structural characteristics of the pump turbine scale model. The friction coefficient of the pipes has been evaluated to be $\lambda = 0.02$ for all the pipes. The determination of the wave speed is described below.

Wave speed determination

The wave speed a for the pipe is given by:

$$a^2 = \frac{1}{\rho\left(\frac{1}{E_{\text{fluid}}} + \frac{1}{A}\frac{\Delta A}{\Delta p}\right)} \qquad (11)$$

Where ρ is the water density, E_{fluid} is the bulk modulus of the water and $A^{-1}\Delta A/\Delta p$ is the rated area increase due to pressure increase. This term can be determined analytically for circular pipes but has to be estimated for pipes having complex cross section. In the case of the pump turbine, the wave speed of the spiral casing and of the distributor are estimated using Finite Element Method -FEM- calculations. The determination of the wave speed of a given cross section of the spiral casing is done in two steps as presented Figure 8:

- distributor channel area increase by assuming a constant pressure in the distributor channel only;
- spiral casing area increase by assuming constant pressure in the spiral casing only.

The FEM analysis is made with the commercial code ANSYS™. First, stay vanes and assembling bolts are considered individually to determine their stiffness. Then, by assuming that each spiral casing part of concern is axisymmetrical, the area increase is determined by including the stiffness of the stay vanes and of the bolts previously determined.

The number of cells in the radial direction of the spiral casing section was set to 3 cells of mesh. This value was determined by comparison of circular pipe wave speed determined by both FEM and analytical calculation. The difference for such geometry was found to be 0.1%. The mechanical properties for the materials of the spiral casing and distributor channels are summarized Table 2.

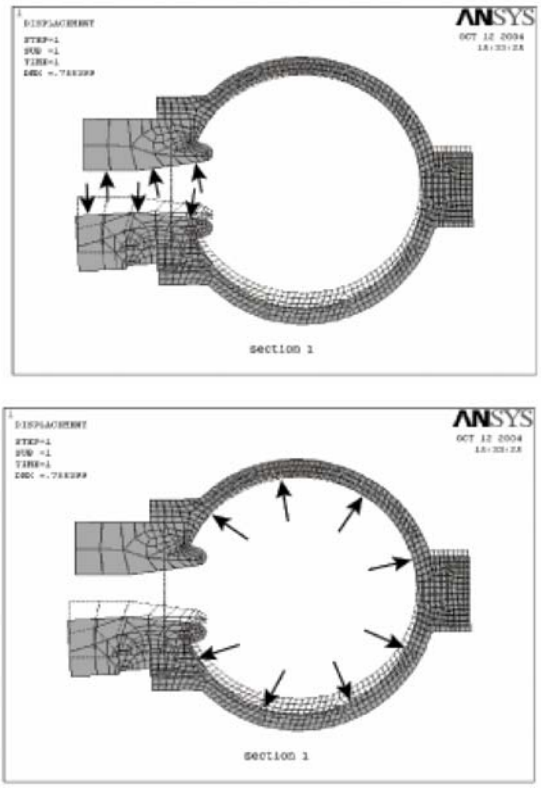

Figure 8 : Determination of the wave speed in the distributor channel (top) and in the spiral casing (bottom).

The spiral casing materials is a composite made of Epoxy resin matrix and glass fiber. The equivalent Young modulus is calculated according to the volume fraction of both components of the composite and by taking into account the main stress direction corresponding to the uniform loading of the hydrostatic pressure. Therefore, the glass fiber Young modulus is calculated according to the fiber cross section area and density corresponding to the main stress direction of concern.

Material	Young Modulus [MPa]	Poisson coeff. [-]
Steel	210	0.27
Bronze	110	0.31
Composite: Epoxy Resin & Glass Fiber	38	0.28

Table 2 : Mechanical properties of spiral casing materials.

For the 4 cross sections defined Figure 5, the corresponding value of the wave speed is calculated, see Figure 9. As expected for a constant spiral casing wall thickness the wave speed is increasing from the inlet up to the tongue as the cross section decreases. For the determination of the wave speed of the 19 elements of the spiral casing model a 2nd order polynomial interpolation is used, see Figure 9.

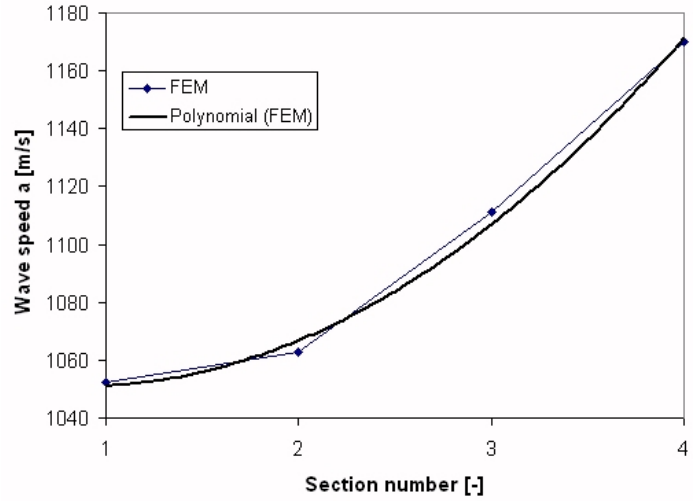

Figure 9 : Wave speed evolution for the 4 cross sections of the spiral casing.

The wave speed of the distributor channels is found to be 800 m/s with small deviation between the 4 sections. The same value is chosen for the wave speed of the impeller blades.

SIMULATION OF THE PUMP TURBINE RSI

The pump turbine scale model of interest is installed on the test rig PF3 of the EPFL Laboratory for Hydraulic Machines. The hydroacoustic model of the test rig is including the pump turbine. A full description of the model of this test rig can be found in [11]. The test rig is made of 2 feedings pumps in series, a piping system, the pump turbine model itself and a downstream tank are presented Figure 10. The chosen operating condition for the simulation of the hydracoustic behavior of the test rig corresponds to the nominal operating point with no cavitation, a discharge of 0.23 m^3/s, a test head of 45 m and a rotational speed of 980 rpm. Each pipe of the spiral casing is considered as 1 element, and each guide vane and impeller vane is modeled with 3 elements. This spatial discretization ensures that a wavelength at the frequency $18\,f_b$ ($k_1 = -2$) is represented by 20 elements. In agreement with the CFL criteria, an integration time step $dt = 85.034\ \mu s$ corresponding to $0.5°$ of impeller rotation is selected. After convergence of the simulation to a periodic behavior, the simulation is continued for 10 impeller revolutions.

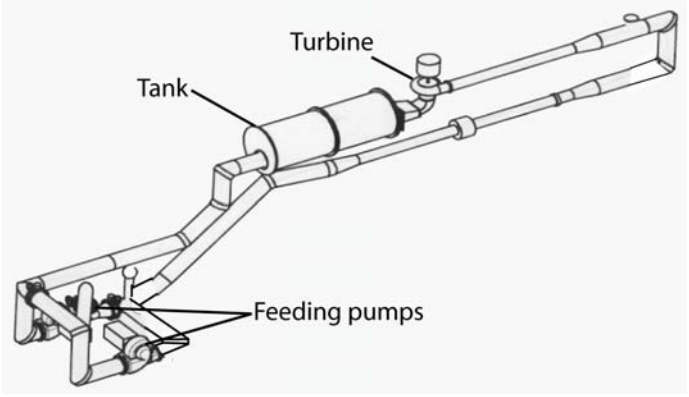

Figure 10 : EPFL test rig PF3.

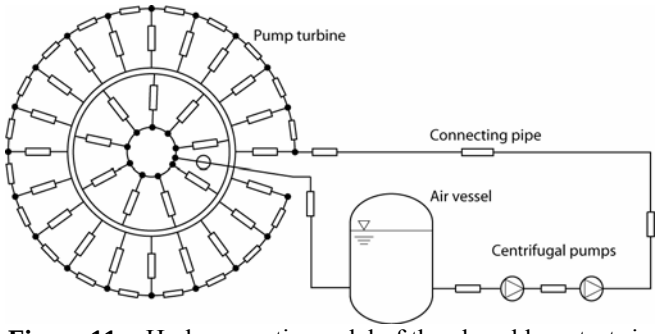

Figure 11 : Hydroacoustic model of the closed loop test rig N°3.

The resulting pressure fluctuations in the spiral casing and in the guide vanes close to the vaneless gap are properly non dimensionalized and presented in a waterfall diagram as a function of the dimensionless frequency f/f_b and the angular coordinate, see Figure 12 and Figure 13. In these diagrams the angular origin is taken at the spiral casing inlet and therefore $\theta = 360°$ correspond to the tongue.

The pressure fluctuation in the vaneless gap, Figure 12, presents significant amplitudes for the expected frequencies $f/f_b = 9,\ 18,\ 27,\ 36,\ 45$, etc. and represents less than 0.5% of the head. The analysis of the phase, not presented here, of these pressure fluctuations shows clearly the diametrical pattern of the pressure mode shapes with for example 2 minima and 2 maxima, i.e. 4π phase shift, for the frequency of $f/f_b = 18$. The pressure fluctuations in spiral casing Figure 13 are characterized by a standing wave for the frequency $f/f_b = 18$ with a wavelength of approximately 4/3 of the spiral casing length. A pressure node is located at $\theta = 150°$ while amplitude maxima take place at $\theta = 20°$ and $\theta = 230°$. This standing wave influences the amplitude of the diametrical mode of the pressure fluctuation in the vaneless gap see Figure 12 .

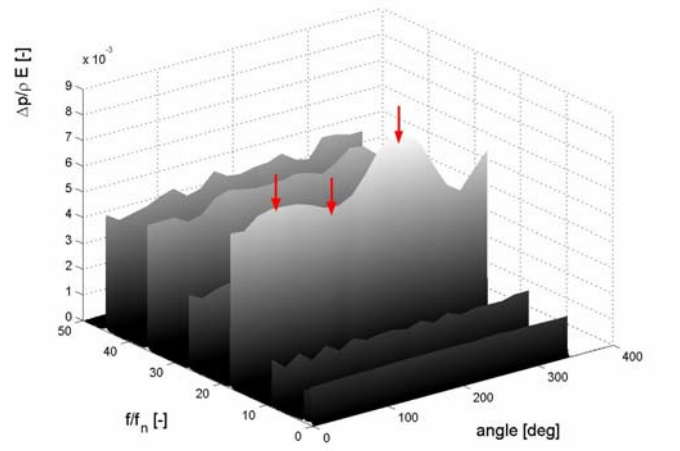

Figure 12 : Waterfall diagram of the pressure fluctuations in the guide vanes close to the vaneless gap.

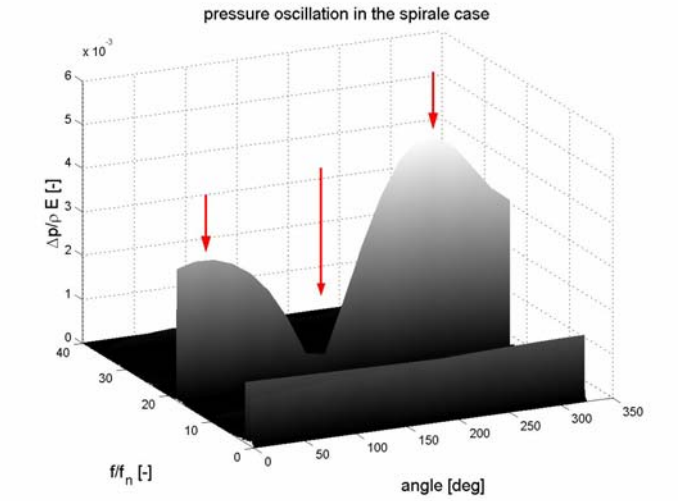

Figure 13 : Waterfall diagram of the pressure fluctuations in the spiral casing.

The patterns of the pressures fluctuations for $k_1 = -2$ are illustrated Figure 14 and Figure 15. The representation is obtained by filtering the time signal of the pressure fluctuations of each spatial node in the pump turbine using a pass band filter around the frequency of interest. For the stationary frame it corresponds to $f/f_b = 18$. In the rotating frame it corresponds to $f/f_b = 20$. The representation is done for the initial time, Figure 14, and for a ¼ period later, Figure 15. The pressure amplitude of every node of the pump turbine is represented on the z axis for the spatial position [x, y] of the node. The bold solid line is the connection between each last node of the guide vane and point out the diametrical mode shape pattern expected for $k_1 = -2$ with 2 maxima/minima. The diametrical mode rotates in the opposite direction of the impeller rotation as predicted by the analytical analysis above. The diametrical mode rotates with a spinning speed of $f_b = -9$. It means that using a pressure transducer in the vaneless gap, the frequency of $f/f_b = 18$ is measured. The interaction between the standing wave in the spiral casing and the diametrical mode are clearly pointed out through the pressure in the guide vanes where pressure fluctuations have similar amplitudes. The results obtained for $k_1 = -4, 5, 7$ show also good agreements with the analytical prediction. However, the $k_1 = 7$ diametrical mode is the last resolvable mode with a resolution of 20 pressure signals. As presented in Figure 13, there is no standing wave in the spiral casing for these frequencies.

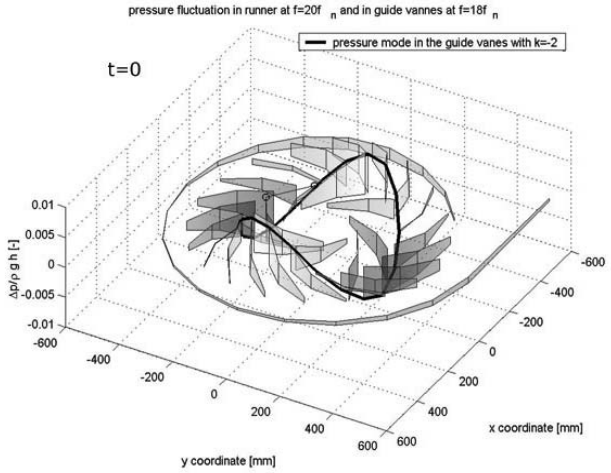

Figure 14 : Pressure fluctuations patterns for $k_1 = -2$, $f/f_b = 18$, $t = 0$.

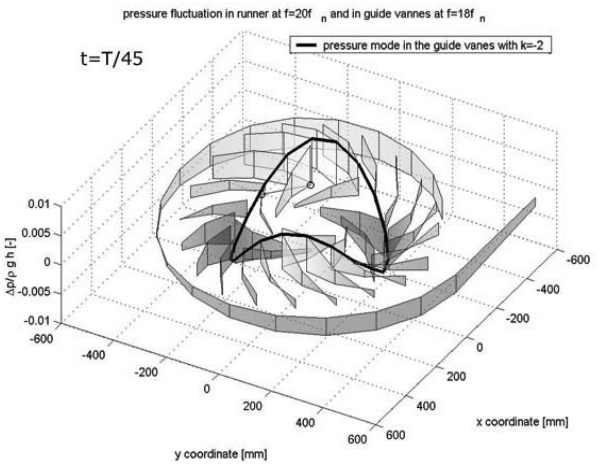

Figure 15 : Pressure fluctuations patterns for $k_1 = -2$, $f/f_b = 18$, $t/T_b = 1/45$.

From these results it can be conclude that hydroacoustic model of the pump turbine allows to obtain and to visualize the RSI pressure fluctuation patterns. Standing wave and diametrical modes are pointed out and corresponding spinning speeds are properly obtained too. The high amplitude of the standing wave in the spiral casing for $k_1 = -2$ is probably related to a natural frequency of the hydraulic system which is close. However, it is important to notice that rotating impeller corresponds to unsteady boundary conditions at the end of the guide vanes. It makes the modal analysis difficult to be done by

using linearized approaches. One of the major advantages of simulating the dynamic behavior of such a system in the time domain is that it offers the possibility to take into account such non-linearities. The modeling based on valve network driven accordingly by the flow distribution between stationary and rotating parts appears to be efficient for the simulation of the hydroacoustic part of the RSI phenomenon. This approach has the advantage to provide also the pressure fluctuations due to RSI in the rotating impeller.

PARAMETRIC STUDY

As the hydroacoustic parameters determination is based on a simplified approach and some parameters are selected arbitrarly, a parametric study is performed in order to assess the sensitivity of the hydroacoustic model to these parameters. Therefore, the influence of the following parameters is investigated in this paragraph:

- blade thickness;
- impeller vane wave speed;
- guide vane wave speed;
- impeller rotating frequency.

The influence of these 4 parameters is investigated considering the frequency, $f / f_b = 18$, mode $k_1 = -2$.

Blade thickness

The model of the excitation is based of the flow distribution between the stationary part and the rotating parts. The resulting discharge law between the 20 guide vanes and the 9 impeller blades can account for the guide vanes and impeller blade thickness. The equivalent thickness of these blades affects the evolution of the connection area between a guide vane and a impeller vane. The Figure 16 presents the 4 possible configurations which are : (A) no blade thickness, (B) consideration of guide vanes thickness only, (C) consideration of impeller blade thickness only and (D) consideration of both guide vanes and impeller blade thickness. The 4 different evolutions of the discharge law of the configurations (A), (B), (C) and (D) are represented on the right part of Figure 16.

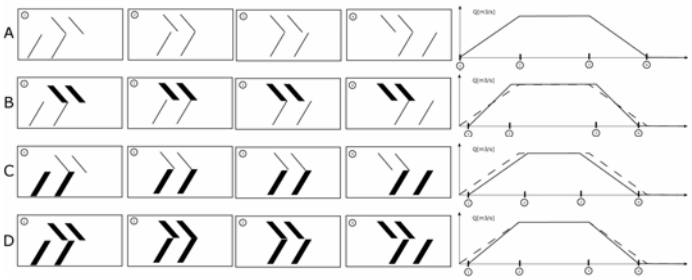

Figure 16 : Discharge law resulting from the guide vanes and impeller blade thickness consideration.

Considering the configurations (B), (C) and (D) 3 series of simulation has been performed considering different blade thickness e. The resulting amplitudes of the pressure fluctuations in the vaneless gap are presented Figure 17. The amplitude corresponding to configuration (B) and (C) provides similar pressure amplitudes in the vaneless gap for identical thickness. The combination of both thicknesses, configuration (D), induces much higher pressure amplitudes. These results show that the higher the blockage effects due to blade thickness, the higher pressure amplitudes in the vaneless gap.

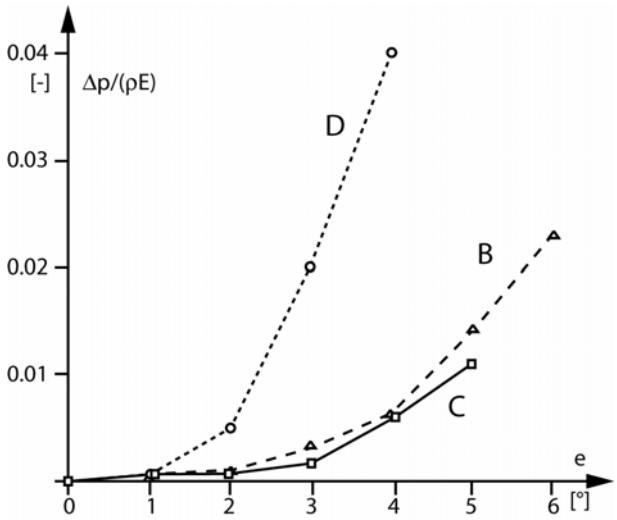

Figure 17 : Pressure fluctuations amplitudes in the vaneless gap for the blade thickness arrangement of Figure 16 for $f / f_b = 18$.

A dynamic pressure amplification factor is used to evaluate the influence between the vaneless gap pressure amplitudes and the amplitudes in the spiral casing. It allows separating the influence of the parameter on the RSI excitation and on the dynamic response of the system. The amplification factor is defined as the ratio between the pressure at any point in the spiral case and the average pressure in the vaneless gap and is expressed as:

$$DA = \frac{p_{\text{spiral}}}{p_{\text{vaneless gap}}} \qquad (12)$$

Figure 18 presents the dynamic amplification factor for 3 different guide vanes thicknesses. It appears that even if the absolute amplitudes of the pressure fluctuations increases, as the excitation in the vaneless gap increases, the dynamic amplification factor remains constant for the 3 tested thicknesses. One interesting consequence of this result is that even if the excitation parameters are arbitrary, the dynamic amplification will be meaningful. It would also means that if the pressure fluctuations can be measured in the vaneless gap during the scale model tests, it could be possible to predict the amplitude of pressure fluctuations in the spiral case.

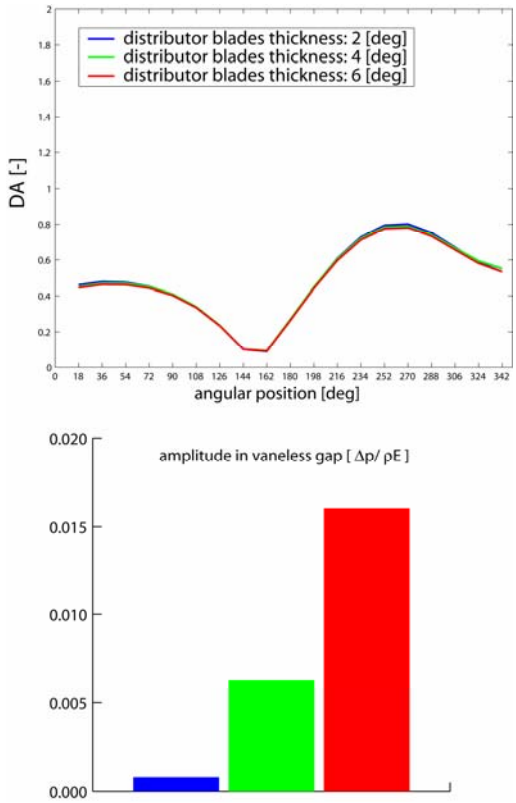

Figure 18 : Influence of the distributor blade thickness on the dynamic amplification between spiral case and vaneless gap for $f/f_b = 18$.

Impeller vane wave speed

The influence of the impeller vane wave speed is investigated by simulating the dynamic behavior of the system considering three different values for this parameter. The chosen values for the impeller wave speed are 700 m/s, 800 m/s and 900 m/s. Figure 19 presents the dynamic amplification factor DA for the 3 different impeller vane wave speeds.

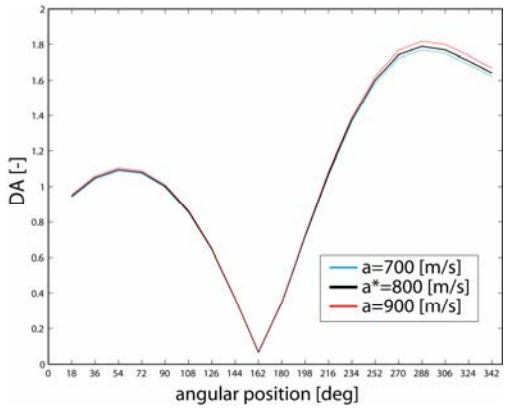

Figure 19 : Influence of the impeller vane wave speed on the dynamic amplification between spiral case and vaneless gap for $f/f_b = 18$.

It is clearly shown that the influence of the impeller vane wave speed is negligible. It means that for pump turbine the combine effect of small vaneless gap and the impeller rotation acts like dead end for such frequency. However, it is right as long as the diffuser remains short compared to the system dimensions.

Guide vane wave speed

4 different values of the guide vane wave speed are chosen to investigate the influence of this parameter on the dynamic amplification between vaneless gap and spiral casing. The chosen values for the guide vane wave speed are 700 m/s, 800 m/s, 900 m/s and 1000 m/s. The resulting dynamic amplification DA and mean value of vaneless gap pressure fluctuation are presented Figure 20.

The mean pressure fluctuation in the vaneless gap remains constant for the 4 cases. However, the dynamic amplification is strongly influenced by the guide vane wave speed. This is related to the fact that traveling time between vaneless gap and spiral casing affects strongly natural frequencies of the hydraulic system. It seems that in this case reducing the guide vane wave speed makes a natural frequency of the hydraulic system closer to $f/f_b = 18$.

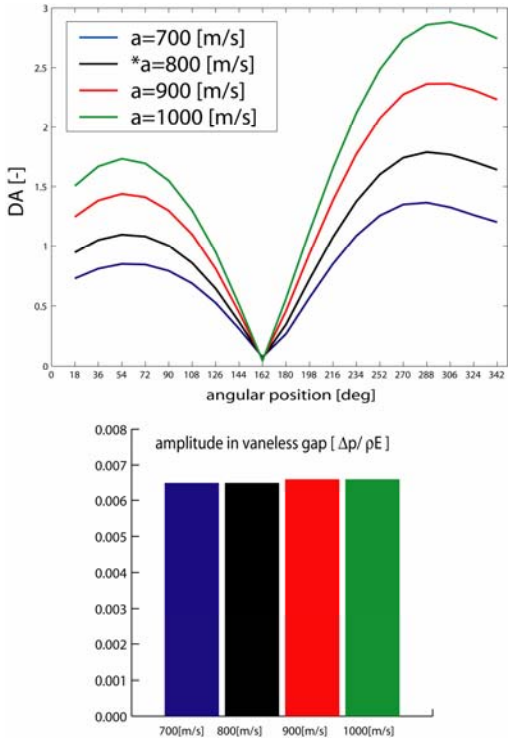

Figure 20 : Influence of the guide vane wave speed on the dynamic amplification between spiral case and vaneless gap for $f/f_b = 18$.

Impeller rotating frequency

4 different impeller rotation speeds are chosen to investigate the influence of this parameter. The chosen values corresponds to $f = 18 \cdot f_b = 292, 296, 300, 304$ Hz. The

resulting dynamic amplification DA and mean value of vaneless gap pressure fluctuation are presented Figure 21.

The impeller rotating speed has strong influence on the dynamic amplification between the vaneless gap and the spiral case. This is due to the change of excitation frequency, which seems to become closer to a natural frequency of the hydraulic system when the rotating frequency decreases. This result is coherent with the influence of the guide vane wave speed. In one case the natural frequency of the hydraulic system increases with the increase of guide vane wave speed, and in the second case the excitation frequency is reduced until it matches the hydraulic natural frequency. However, in both cases the amplitude of the pressure fluctuations in the vaneless gap remains constant.

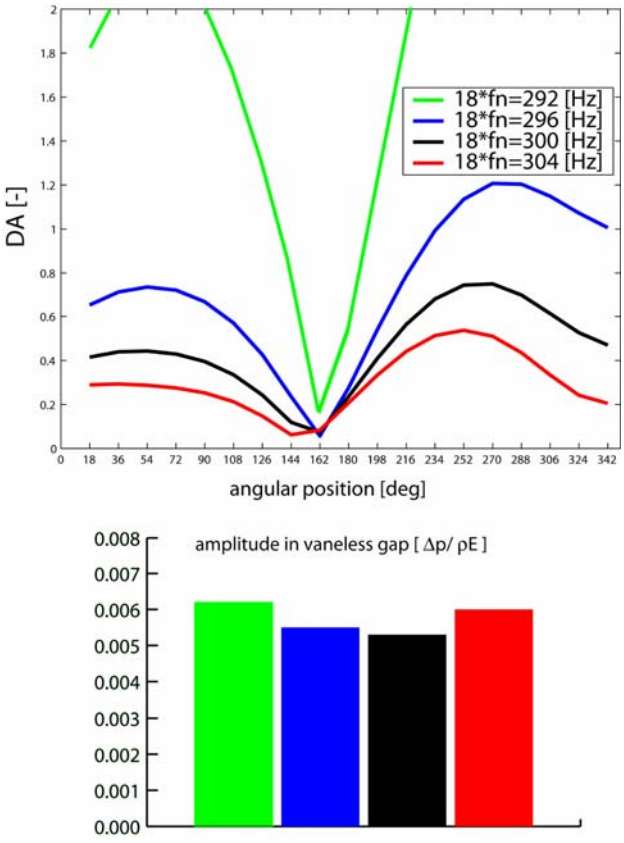

Figure 21 : Influence of the impeller rotating speed on the dynamic amplification between spiral case and vaneless gap for $f/f_b = 18$.

CONCLUSION

Rotor stator interaction in Francis pump turbine may causes strong pressure fluctuations in the vaneless gap between the guide vanes and the impeller blades characterized by rotating diametrical mode shapes that can excite natural frequency of the hydraulic system and resulting in standing wave in the spiral casing. These 2 effects can induce resonance with mechanical or concrete structure jeopardizing the security of the power plant.

This paper presents a new approach for the modeling of the hydroacoustic part of the phenomenon. A one-dimensional simulation model of Francis pump turbine is set up according to the topology of a 20 guide vanes and 9 impeller vanes pump turbine. The hydroacoustic parameters of the model are determined from the geometrical and structural characteristics of the machine and the test rig.

The resulting RSI model comprises a network of 180 valves connecting each guide vane with each impeller vane. The valve opening functions are driven accordingly with the flow distribution between the stationary part and the rotating parts. The analysis of the pressure fluctuations resulting from the rotor stator excitation shows that RSI patterns like rotating diametrical pressure mode and standing wave are properly simulated. Influence of the standing wave on the diametrical pressure mode is pointed out. The chosen excitation model appears to be realistic for the investigation of hydroacoustic part of the RSI.

Moreover, a parametric study investigating the influence of blade thickness, impeller blades and guide vane wave speed and impeller rotating speed is carried out. It results that the wave speed in the impeller blades has not significant influence. The influence of guide vane wave speed and impeller rotating frequency tends to show that the amplitude of the standing wave in the spiral casing for the frequency $f/f_b = 18$ is strongly affected by these parameters because of the closeness a natural frequency of the hydraulic system.

Overall, this model gives satisfactory qualitative results and needs to be validated experimentally. However, if the dynamic amplification gives reliable trends, the determination of the absolute pressure fluctuations amplitudes is more challenging. The excitation model is based on the flow distribution between the stationary parts and the rotating parts of the machine and is arbitrary. Its parameters are only related to connection area between guide vanes and impeller blades evolution due to impeller rotation. To obtain a more reliable quantitative result, the excitation model should be improved and be able to take into consideration all the parameters affecting RSI like the gap amplitude, the wake angle of the impeller blade and the blades thickness etc. This could be achieved through the coupling of a one-dimensional code like SIMSEN for the modeling of the hydraulic system with a CFD tool for the modeling of the RSI excitation. This approach seems realistic regarding the negligible influence of the impeller hydroacoustic parameters.

ACKNOWLEDGMENTS

The authors would like to thank particularly all the partners of the HYDRODYNA Eureka Project No 3246, i. e. ALSTOM Hydro, EDF-CIH, GE Hydro, VA TECH Hydro, VOITH-

SIEMENS Hydro Power Generation for their financial support and assistance. The HYDRODYNA project is funded by the CTI, Swiss Federal Commission for Technology and Innovation, Contract award No 7045.2 EUS. For this paper, the authors took advantages of the development of the SIMSEN hydraulic extension, developed in collaboration with P. Allenbach, Dr. A. Sapin, and Prof. J.-J. Simond from the EPFL Laboratory for Electrical Machines under the following contract awards: CTI No 5750.1 EBS, PSEL No 215 Scapin, EDF-CIH, HMD 420.210.3459.

REFERENCES

[1] Bolleter, U., 1988, "Blade passage tones of centrifugal pump. ", Vibrations, Vol. 4, No 3, pp. 8-13.

[2] Chen, Y. N., 1961, "Water-Pressure Oscillations in the Volute Casings of Storage Pumps.", Sulzer Technical Review, Research Number, pp. 21-34.

[3] Den Hartog, J. P., 1956, "Mechanical vibrations.", 4th edition, New York, McGraw-Hill pp. 7-9.

[4] Dörfler, P., 1984, "On the phase role of phase resonance in vibrations caused by blade passage in radial hydraulic turbomachines.", Proceedings, 12th IAHR Symposium, Stirling, paper 3.3, pp. 227-241.

[5] Franke, G., Powell, C., Seidel, U., Koutnik, J., Fischer, R., 2005, "On pressure mode shapes arising from rotor/stator interactions.", Sound & Vibration, March 2005, pp. 14-18.

[6] Fischer, R., Powell, C., Franke, G., Seidel, U., Koutnik, J., 2004, "Contributions to the improved understanding of the dynamic behaviour of pump turbines and uses thereof in dynamic design.", Proceedings, 22nd IAHR Symposium, Stockholm, paper B11-3.

[7] Gonzalez, J., Fernandez, J., Blanco, E., Santolaria, C., 2002, "Numerical simulation of the dynamic effects due to impeller-volute interaction in a centrifugal pump. ", Trans. ASME, J. Fluids Eng., vol. 124, pp. 348-355, June 2002.

[8] Haban, V., Koutnik, J., Pochyly, F., 2002, "1-D Mathematical model of high-frequency pressure oscillations induced by RSI including an influence of fluid second viscosity.", Proceedings, 21st IAHR Symposium, Lausanne, pp. 735-740.

[9] Moregenroth, M., Weaver, D. S., 1998, "Sound generation by a centrifugual pump at blade passing frequency", ASME, J. Fluids Eng. Vol. 120, pp. 736-743, October 1998.

[10] Nicolet, C., Avellan, F., Allenbach, P., Sapin, A., Simond, J.-J., 2002, "New Tools for the Simulation of Transient Phenomena in Francis Turbine Power Plants". Proceedings of the 21st IAHR Symposium, Lausanne, pp. 519-528.

[11] Nicolet, C. , Arpe, J., Avellan, F., 2004 "Identification and Modeling of Pressure Fluctuations of a Francis Turbine Scale Model at Part Load Operation ". Proceedings of the 22nd IAHR Symposium on Hydraulic Machinery and Systems, Stockholm, Sweden.

[12] Parrondo-Gayo, J. L., Gonzalez-Perez, J., Fernandez-Franco, 2002, "The effect of the operating point on the pressure fluctuations at blade passage frequency in the volute of a centrifugal pump. ", Trans. ASME, J. Fluids Eng., vol. 124, pp. 348-355, September 2002.

[13] Ohura, Y., Fujii, M., Sugimoto, O., Tanaka, H., Yamagata, I., 1990, "Vibration of the powerhouse structure of pumped storage power plant.", Proceedings, 15th IAHR Symposium, Belgrade, section U2.

[14] Paynter, H. M., 1953 "Surge and water hammer problems". Transaction of ASCE, vol. 146, p 962-1009.

[15] Tanaka, H., 1994, "Special design considerations for ultra high head pump-turbines.", Hydropower & Dams, November 1994, pp. 107-112.

[16] Wylie, E. B. & Streeter, V.L., 1993, "Fluid transients in systems". Prentice Hall, Englewood Cliffs, N.J.

